THE ASTROPHYSICAL JOURNAL, 364:433–443, 1990 December 1

A SEARCH FOR SMALL-SCALE X-RAY SURFACE BRIGHTNESS FLUCTUATIONS IN CLUSTERS OF GALAXIES

ANDRZEJ SOLTAN AND DANIEL G. FABRICANT
Harvard-Smithsonian Center for Astrophysics
Received 1990 April 6; accepted 1990 May 31

ABSTRACT

A search for small-scale structure in the X-ray surface brightness of 20 nearby ($z \leq 0.036$) clusters of galaxies is described. Our technique is to compare 0.3–3.5 keV observations made with the Imaging Proportional Counter (IPC) aboard the *Einstein Observatory* to detailed simulations of intrinsically smooth clusters. The simulations include modulations introduced by the IPC and background/foreground X-ray sources. Each cluster is divided into ~four radial zones for analysis. We divide these radial zones into two subsamples (each containing 38 zones) on the basis of total detected IPC counts; we refer to these as the low-count and high-count samples. The rms fluctuations due to counting statistics alone are typically in the range of 10%–30% in the high-count sample. We detect excess fluctuations of 1′ scale in the high-count sample, but none in the low-count sample. The excess fluctuations in the high-count sample could be produced by ~one source per zone emitting at $\sim 4 \times 10^{41}$ ergs s^{-1} in soft X-rays. We suggest that low-luminosity active nuclei in the cluster galaxies or a hot interstellar medium retained by some galaxies are the most likely origins of this emission.

Subject headings: galaxies: clustering — galaxies: nuclei — galaxies: X-rays

I. INTRODUCTION

Einstein Observatory soft X-ray images of galaxy clusters with a bimodal X-ray surface brightness distribution (Forman *et al.* 1981) rewakened interest in the problem of substructure in galaxy clusters. Since that time, X-ray and optical studies have established that ~30%–40% of clusters contain multiple condensations of galaxies with characteristic separations of ~1 Mpc which are also traced by the 10^7–10^8 K X-ray emitting gas that pervades the clusters (e.g., Geller and Beers 1982; Dressler and Shectman 1988; Jones and Forman 1990).

However, the uniformity of the X-ray emission on small scales has rarely been probed. Looking through the *Einstein Observatory* Imaging Proportional Counter (IPC) images cataloged by Jones and Forman (1990), one forms the impression that many clusters have irregular surface brightness profiles. However, counting statistics, detector modulations, and background sources undoubtedly contribute to this subjective reaction, and a quantitative approach is required for a secure assessment. The strongest small-scale (tens of kpc or less) nonuniformities might be expected to arise from the hot interstellar medium of individual galaxies and low-luminosity active galactic nuclei (AGN). Emission from blobs of gas at lower temperature and higher density associated with cooling flows and galaxy ejecta might be visible as well. This emission would not necessarily be associated with individual galaxies in the cluster. With sufficient sensitivity, beyond that available with the *Einstein Observatory*, the integrated emission from discrete X-ray sources within the cluster galaxies might be detectable. The measurement of the small-scale fluctuations in the cluster emission are of further importance insofar as they affect measurements of the cluster mass distribution and attempts to measure the distance scale by means of the Sunyaev-Zeldovich effect.

As a result, we have undertaken the present search for small-scale surface brightness features in a sample of nearby clusters observed in soft X-rays with the *Einstein* satellite. Although it would clearly be desirable to be able to distinguish between low-luminosity active nuclei and a hot interstellar medium on the basis of the source extent, we have used data from the IPC with ~1.′4 FWHM spatial resolution as opposed to the High Resolution Imager (HRI) with ~3″ resolution. The primary reason for this choice is that the IPC was used to observe approximately twice the number of nearby clusters observed with the HRI. In addition, the spatial nonlinearities of the IPC are better understood, as are the contributions of background sources (e.g., Gioia *et al.* 1990). Finally, although the sensitivity of the IPC for point sources is slightly less than that of the HRI, its sensitivity for sources with 1′ extent is about an order of magnitude greater.

X-ray emission associated with individual galaxies in the Virgo Cluster and in A1367 has been reported previously. Bechtold *et al.* (1983) used very deep (65,000 s integration) HRI observations of A1367 at $z = 0.0213$ to search for sources with scale less than or equal to 2′ superposed on a smooth cluster emission. They detected three unresolved and nine extended sources which they identified with cluster galaxies (types E to Sa), as well as five unresolved and six extended sources not coincident with cluster galaxies. Three of the extended sources have subsequently been identified with background clusters of galaxies (Forman and Jones 1990). The 0.5–4.5 keV luminosities of the sources identified with cluster galaxies range between $4 \times 10^{40}$and 2.4×10^{42} ergs s^{-1} for the point sources and 1.7×10^{41} and 6.5×10^{41} ergs s^{-1} for the extended sources. Bechtold *et al.* suggest that the extended X-ray emission associated with the cluster galaxies most plausibly arises from hot gas ($kT \sim 1$ keV) gravitationally bound to the galaxies.

Canizares, Fabbiano, and Trinchieri (1987) have pointed out that as a group, the A1367 galaxies with extended X-ray emission have a considerably higher ratio of X-ray to optical luminosity than do galaxies in the Virgo Cluster and in the field. On this basis, they suggest that these sources may not be associated with individual galaxies but may instead be markers of local maxima in the irregular cluster emission. Canizares (1988)

reports 3 σ upper limits for 24 early-type galaxies in the Coma Cluster (A1656) in the range 3×10^{40} to 3×10^{41} ergs s^{-1} in the 0.2–3.5 keV band. Canizares concludes that the soft X-ray emission of galaxies in rich clusters is not uniformly enhanced with respect to field and Virgo Cluster galaxies. However, A1367 represents an environment intermediate between the extremes of the Coma and Virgo Clusters, so the results of Bechtold *et al.* and Canizares are not necessarily in conflict. Furthermore, since the luminosities of the sources in A1367 are quite uncertain (the detections are at typically 3–4 σ), the gap between Bechtold *et al.*'s detections and Canizares's upper limits is not large.

The frequency of low-luminosity ($L_x \leq 10^{43}$ ergs s^{-1}) AGN in either field or cluster galaxies is poorly understood. Elvis, Soltan, and Keel (1984) have suggested that X-ray emission from low-luminosity AGN might account for $\sim$20% of the 2–10 keV X-ray background; Persic *et al.* (1989) suggest that an upper limit of $\sim$15% is appropriate. These estimates of X-ray emission from low-luminosity AGN are quite uncertain because they rely on predicting the X-ray luminosity from the Hα luminosity of galaxy nuclei. The scatter in $L_x/L_{H\alpha}$ is large. Elvis, Soltan, and Keel derive a mean value for $L_x/L_{H\alpha}$ of 40 (for the 2–10 keV X-ray band) from a sample of Seyfert galaxies with L_x typically greater than 10^{43} ergs s^{-1}. Halpern and Steiner (1983) give 0.5–4.5 keV X-ray and Hα luminosities for 12 LINER galaxies (low ionization nuclear emission-line regions) with X-ray luminosities between 10^{40} and 3×10^{43} ergs s^{-1}. The mean value of $L_x/L_{H\alpha}$ is 21 (0.5–4.5 keV X-ray band) for their sample. Furthermore, the distribution of nuclear Hα luminosities as a function of absolute galaxy magnitude have been determined from relatively small surveys of nearby, bright galaxies (e.g., Keel 1983; Heckman 1980). Unfortunately, the dependence of activity in the nuclei of galaxies upon Hubble type and local galaxy density is poorly understood. Dressler, Thompson, and Shectman (1985) find that galaxies with emission-line spectra are less prevalent in rich clusters of galaxies than in field galaxies, but it is difficult to directly compare their sensitivity limits with those of Keel and Heckman. If we follow Elvis, Soltan, and Keel and assume that the distribution of Hα luminosities is independent of Hubble type (and environment), but modify their Table 1 to use the $L_x/L_{H\alpha}$ relationship from Halpern and Steiner, we calculate (with considerable uncertainty) that $\sim$25% of galaxies with $M_p \leq -19.5$ (or $\sim M_B$) would have 0.5–4.5 keV X-ray luminosities greater than 10^{41} ergs s^{-1}. It would be advisable to view this as an upper limit given the results of Dressler, Thompson, and Shectman. As described below, this luminosity is large enough to be of interest for the *Einstein* data.

The observability of clumps of cooler gas associated with galaxy ejecta and cooling flows has not been addressed theoretically to our knowledge, nor have relevant observations been made. Perhaps the only way of making significant progress is to find clear-cut local peaks in the X-ray surface brightness not associated with cluster galaxies or background sources. This is not possible with the present data, as will become apparent below.

For spiral galaxies and low-luminosity early-type galaxies ($M_B \leq -19.5$), the X-ray emission is thought to be predominantly the integrated emission from supernova remnants and X-ray binaries. (See Fabbiano 1989 for a review of the X-ray emission from normal galaxies.) Assuming that cluster membership does not affect the luminosity of these sources, their contribution for a typical cluster galaxy ($M_B \leq -20.5$), would be less than or equal to 10^{40} ergs s^{-1} in soft X-rays, below the sensitivity of the present study. For optically luminous early-type galaxies ($M_B \geq -19.5$), the contribution from hot gas (frequently termed a hot interstellar medium) becomes increasingly important, although the effect of a cluster environment remains controversial as discussed above.

In § II we describe the sample of clusters chosen for study. The preparation of the data and the simulations that are required by our analysis technique are described in § III. The details of the surface brightness fluctuation analysis are presented in § IV. Section V summarizes the results of the fluctuation analysis, while § VI discusses the physical significance of the results.

II. DEFINITION OF THE CLUSTER SAMPLE

The observations of the clusters of galaxies used for this study were selected from archival IPC data. In order to minimize as far as possible the selection biases resulting from incomplete sky coverage and the variable exposure times characteristic of the *Einstein* observations, the study is limited to nearby clusters, drawn (with three exceptions) from the Abell catalog (Abell 1958). Our sample includes those clusters and groups of galaxies at $z \leq 0.036$ with high enough luminosity and sufficient exposure with the *Einstein Observatory* to allow a detailed look at surface brightness fluctuations in the extended cluster X-ray emission. Clusters without well-detected extended emission have not been included in the sample; only observations with at least 6 counts arcmin^{-2} over a region of at least 5′ in radius are used. This criterion imposes a low-luminosity cutoff at about 10^{43} ergs s^{-1} in the 0.3–3.5 keV energy band. (Luminosities are estimated assuming that 1 IPC count in pulseheight channels 3–10 corresponds to 3.4×10^{-11} ergs cm^{-2} in this energy band, after correction for interstellar absorption in our Galaxy. This conversion factor is correct for a thermal spectrum with $kT \geq 4$ keV and absorption equivalent to a hydrogen column of 3×10^{20} cm^{-2}. The conversion factor varies by less than 20% for thermal spectra with $1 < kT < 8$ keV and power law spectra with a photon index between 1 and 2. If the interstellar absorption is increased by an order of magnitude, the conversion factor increases by $\sim$50%.) Our sample includes 17 of the 31 Abell clusters with distance class ≤ 3 at $z \leq 0.036$, as well as the group AWM 7, the Zwicky cluster ZW 1615+35, and the cluster surrounding the radio source 3C 129. The X-ray morphologies of the latter three clusters are indistinguishable from those of the Abell clusters. Table 1 summarizes some basic data for the clusters in the sample: the position of the IPC field center, the galactic latitude, the cluster redshift, the exposure length, and the 0.3–3.5 keV cluster X-ray luminosity integrated over the central portion (32′ × 32′) of the IPC field. Of the remaining 14 Abell clusters at $z \leq 0.036$ not included in the sample, two were not observed by *Einstein* (A1228 and A1257) and 12 failed to meet the total count criterion described previously. To avoid the complication of dealing with areas partially vignetted by the IPC window support structure, only the central region of the IPC (32′ × 32′) was used. A Hubble constant of $H_0 = 50$ km s^{-1} Mpc^{-1} is used throughout.

III. DATA PREPARATION AND SIMULATED OBSERVATIONS

The objective of this study is to search for small-scale surface brightness fluctuations about a smoothly varying cluster profile using pixel to pixel count rate fluctuations. However, significant contributions to the observed fluctuations arise

TABLE 1

THE CLUSTER SAMPLE

Cluster	α (1950.0)	δ (1950.0)	b	z	Exposure	L_x ergs s^{-1}
A194	1^h23^m0	$-1°46'$	$-63°$	0.0186	9779s	1.1×10^{43}
A262	1 49.9	35 55	−25	0.0164	3979	5.1×10^{43}
AWM 7	2 51.3	41 23	−16	0.0176	778	1.5×10^{44}
A400	2 55.0	5 50	−45	0.0232	10842	2.9×10^{43}
A426	3 16.5	41 20	−13	0.0183	16035	9.5×10^{44}
A496	4 31.4	−13 21	−36	0.0316	6179	2.9×10^{44}
3C 129	4 46.1	44 58	0	0.0218	7121	8.5×10^{43}
A539	5 14.2	6 25	−18	0.0205	3706	3.6×10^{43}
A1060	10 34.5	−27 16	27	0.0114	10851	3.6×10^{43}
A1185	11 8.2	28 57	68	0.0304	11857	2.9×10^{43}
A1314	11 32.1	49 20	64	0.0341	6639	4.6×10^{43}
A1367	11 41.9	20 7	73	0.0213	24711	1.4×10^{44}
A1656	12 57.3	28 12	88	0.0235	8744	7.0×10^{44}
	12 57.3	27 52	...	...	6686	
	12 57.3	28 38	...	...	6659	
A1736	13 24.7	−26 55	35	0.035	10660	1.1×10^{44}
A2052	15 14.3	7 12	50	0.0345	1480	2.3×10^{44}
A2063	15 20.6	8 49	50	0.0337	3937	1.9×10^{44}
A2147	16 0.0	16 3	44	0.0356	10484	3.6×10^{44}
ZW 1615+35	16 15.7	35 8	46	0.0321	8319	3.1×10^{43}
A2199	16 26.9	39 38	44	0.0305	4902	4.2×10^{44}
A2634	23 36.0	26 45	−33	0.0322	22524	1.1×10^{44}

from a number of sources external to the cluster: superposed background or foreground sources, instrumental imperfections, and statistical noise. In order to determine the level of fluctuations intrinsic to a given cluster, the observed count variations have been compared with those in simulated observations of smooth clusters with large-scale surface brightness profiles similar to the real clusters.

The reprocessed *Einstein* data are used for this study; the temporal gain changes and the large-scale spatial gain variations of the IPC have been removed by mapping the raw pulse-height channels to a reference set of pulse-height channels corresponding to an intermediate detector gain (see Harnden *et al.* 1984). Data in channels 3–10 in the remapped system are used in this study, with nominal X-ray energy boundaries of 0.3–3.5 keV. The IPC pixels have been binned 8 × 8, resulting in analysis pixels 64″ on a side. No background is subtracted and no vignetting correction is applied to the raw data. For the purposes of the subsequent analysis, each observation consists of X-ray counts in an array of $\sim 30 \times 30$ elements.

The simulated clusters that will be compared to the *Einstein* observations have surface brightness distributions of the form:

$$f \sim [1 + (r/r_c)^2]^{-3\beta+1/2} + f_0 \,. \quad (1)$$

The parameters of the model r_c, β, and f_0 have been chosen to provide the best description of the observed clusters by minimizing χ^2. The constant term f_0 is included to allow for variations about the nominal background level. For clusters with noticeably elliptical X-ray isophotes, two additional parameters are introduced: ellipticity (assumed to be independent of radius) and the position angle of the major axis. To allow greater accuracy, the simulations are performed using 16″ pixels, which as a final step are binned 4 × 4 for comparison with the observations.

a) Foreground and Background Sources

In order to account for foreground and background sources, unresolved sources are added to mimic the population of sources found in the Deep and Medium Sensitivity Surveys (MSS) conducted with the *Einstein Observatory*. The MSS uses only data for galactic latitudes $|b| \geq 20°$. The actual number and fluxes of the sources in a particular simulation are random variables drawn from analytic fits to the distribution of the X-ray source counts (Gioia *et al.* 1984, 1990). The number of extragalactic objects per steradian with fluxes that exceed S are well represented by a power law:

$$N(>S) = KS^{-\alpha} \,. \quad (2)$$

With the flux in units of ergs cm^{-2} s^{-1} in the 0.3–3.5 keV energy band, $\alpha = 1.45$ and $K = 2.4 \times 10^{-15}$. These coefficients are determined over the range of fluxes between 7×10^{-14} to 1×10^{-11} ergs cm^{-2} s^{-1}. (We use the number counts of Gioia *et al.* 1984; the work reported here was carried out before the completion of the extended survey of Gioia *et al.* 1990. The results from the extended survey are very similar.) Extrapolation to the Deep Survey limit of $\sim 4.5 \times 10^{-14}$ ergs cm^{-2} s^{-1} gives 16.2 sources deg^{-2}. Gioia *et al.* find that galactic sources constitute 25% of the X-ray sources in the EMSS. We therefore increase the normalization (K) by a factor of 1.33 to account for galactic sources at high galactic latitude, making the assumption that they follow the same power-law slope as the extragalactic sources at fluxes above the Deep Survey limit. Only sources with fluxes above the Deep Survey limit are added in this fashion; the contribution from sources below this limit and from the non–X-ray background is added separately, estimated from the average of six Deep Survey fields with the detected sources removed. Note that the fluctuations due to sources below the Deep Survey limits will be underestimated due to the summation over six fields. However, the fluctuations due to undetected sources below the Deep Survey limit are smaller than those due to sources above this limit by a factor of ~ 30.

We note that two of the 20 clusters in our sample lie at significantly lower latitudes than the 20° cutoff of the MSS: A426 at $l = 151°$, $b = -13°$ and 3C 129 at $l = 161°$, $b = 0°$.

Hertz and Grindlay (1984) present the results of a low Galactic latitude ($|b| \leq 15°$) X-ray source survey using the *Einstein* IPC. The flux limit of this survey is comparable to that of the MSS. Although the low-latitude survey shows an excess of sources toward the bulge of our Galaxy, the source counts in the neighborhood of the Galactic anticenter (where A426 and 3C 129 lie) are consistent with the high-latitude MSS results, although the errors are large. We have elected to leave these clusters in our sample and calculate the contribution from foreground and background sources using the MSS source counts. Only $\sim 5\%$ of the regions in our final high count sample (which excludes A426 as discussed below) lie at Galactic latitudes $\leq 15°$.

The point response function of the IPC and *Einstein Observatory* mirror combination is approximated by a two-dimensional Gaussian distribution with $\sigma = 38''$; the simulated background sources are given this profile. The distribution of counts from the simulated cluster and background and foreground sources is then modified to account for the vignetting of the *Einstein* telescope of-axis. An analytic approximation for the vignetting, as given in Harnden *et al.* (1984) is used. The vignetting is $\sim 23\%$ 16′ off-axis. The accuracy of the vignetting correction does not affect the simulated cluster profiles since any error is absorbed in the model profile.

b) Instrumental Modulations

The most important instrumental sources of fluctuations in the observed surface brightness are spatial variations of the detector gain and nonlinearities in the detector positional readout. (The algorithm which removes scale changes over the IPC unfortunately introduces additional small-scale nonlinearities.) As a result of these two effects, modulations with a characteristic scale of $\sim 1'$ are introduced. These modulations are well approximated by the product of two separable functions, each depending on the position along one of the two detector axes. (The gain variations are caused by wire to wire spacing variations and the scale correction is performed independently in each axis.) Because these modulations are an important potential source of systematic errors, the procedure used to create a modulation map from the Deep Survey observations is described below in detail.

Let $f(y, z)$ denote the surface brightness distribution incident on the IPC at the focal plane of the X-ray mirror. The surface brightness distribution $f_{obs}(y, z)$ recorded by the IPC is given by the equation:

$$f_{obs}(y, z) = g_y(y) \times g_z(z) \times f(y, z) , \quad (3)$$

where the functions g_y and g_z describe the detector modulations. The distributions g_y and g_z have been determined from six summed, source-subtracted Deep Survey observations that were processed without aspect corrections to avoid blurring the detector modulations. The total exposure in the six fields is $\sim 278{,}000$ s. The factorization has the beneficial side effect that the modulations from faint, undetected sources in the Deep Surveys are effectively averaged out. All detected sources are removed prior to the co-addition, and the appropriate corrections for exposure are made. The vignetting of the X-ray background and large-scale nonuniformities in the non–X-ray background have been removed by fitting to a second-order polynomial.

Our analysis below uses the second moment of the photon distribution. The observed fluctuations in the projected distributions g_y and g_z are increased by the effects of counting statistics and fluctuations along the perpendicular axes. The contribution from these effects has been estimated directly from the second moment of the pixels contributing to each 16″ wide bin in the projected distributions, and the average contribution for each axis is subtracted in quadrature from the observed fluctuations. The amplitude of the corrected fluctuations is $\sim 10\%$ less than the observed fluctuations. The corrected functions g_y and g_z, binned with 32″ resolution, are plotted in Figure 1.

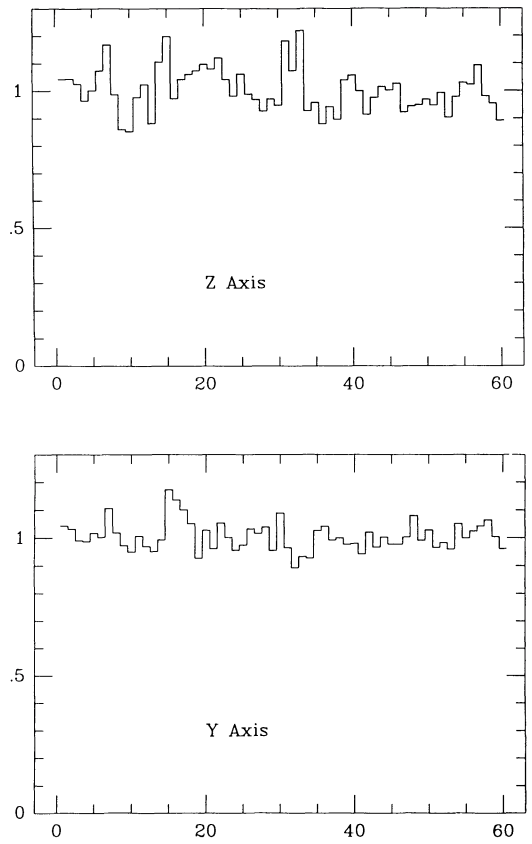

FIG. 1.—A plot of the functions g_y and g_z, the one-dimensional projections of the small-scale modulations introduced by the IPC. Data from the central 32′ of the IPC are plotted in 32″ bins. The data have been divided by a second order polynomial to remove vignetting due to the *Einstein Observatory* mirror. The distributions have been normalized to an average value of 1.

If the IPC data are binned into 64″ pixels, statistical fluctuations in the summed Deep Survey fields allow the IPC modulations to be determined to $\sim 3\%$ accuracy. Thus the systematic errors in the fluctuation analysis will be of this order. However, except for the central regions of the Perseus Cluster, counting statistics in the cluster observations dominate. Small fluctuations of the telescope pointing around the average position tend to smooth out the detector modulation pattern after aspect corrections are applied. This pointing jitter averages ~ 0.2; the largest jitter encountered in these observations is ~ 0.7. This effect is accounted for in the simulations of the individual clusters using aspect data.

Because the modeling of the detector modulations is crucial to the whole fluctuation analysis, we have attempted to check our results from the summed Deep Surveys using data obtained in preflight tests of the IPC. In one such test, the IPC was uniformly illuminated with aluminum K X-rays at 1.49

keV. During this test, $\sim 3 \times 10^4$ photons were collected in the central $32' \times 32'$ of the IPC. The comparison between these data and the Deep Survey data is interesting for three reasons: the data were acquired at widely separated times, the incident spectra are quite different, and the preflight data are not contaminated with X-ray sources.

The preflight data from the central region of the IPC were binned into 900 pixels (64″ on a side) containing an average of 34.39 counts. The functions g_y and g_z determined from the Deep Survey fields were used to predict the counts in each pixel, normalizing to the average count level. The rms difference between the preflight data and the predicted modulations is 5.94 counts. Adding the statistical contributions from the preflight data (5.86 counts) and the Deep Survey map (3% or 1.03 counts) in quadrature, we obtain 5.95 counts for the expected statistical contribution to the rms difference, in excellent agreement with the measurement.

We define an average detector modulation as the rms of the photon distribution (corrected for Poisson noise) divided by the average number of counts per pixel. For the preflight test this quantity is 0.077 ± 0.010 using 64″ pixels. In the summed Deep Survey observations there are $\sim 9.7 \times 10^4$ counts in the central $32' \times 32'$. The average detector modulation in the modulation map determined from the projections of the Deep Survey data is also 0.077 ± 0.005, in fortuitously good agreement. If the functions g_y and g_z are displaced in y or z by one or two pixels from their correct positions, the rms difference between the preflight data and the normalized product of g_y and g_z increases sharply. When such an offset is introduced, a residual of ~ 2.5 counts per pixel remains in the rms difference after subtraction of the statistical contribution in quadrature. This residual ($\sim 7\%$ of the mean count per pixel) difference is comparable to the rms difference expected for two uncorrelated modulation patterns. We conclude that the IPC spatial modulations are stable with time and do not strongly depend on the spectrum of the incident counts. This conclusion is also reached by Wu *et al.* (1990). Wu *et al.* have produced a modulation map with excellent statistics from 400 IPC observations, subtracting the contributions from point sources in each case. The modulation functions g_y and g_z plotted in Figure 1 agree in detail with the projected distributions given in Figure 3 of Wu *et al.*

c) *Statistical Noise*

In the last step of the simulations Poisson fluctuations are added to the simulated cluster images and the simulated data are binned in the same way as the real observations. For each cluster 100 simulations have been performed.

IV. THE FLUCTUATION ANALYSIS

a) *Definition of the Technique*

To assess the surface brightness fluctuations in a given region, we calculate the mean square difference (pixel by pixel) between the observed and the predicted number of counts obtained from fits to the smooth cluster emission using equation (1). The parameters r_c, β, and f_0 are fixed by fits to the whole cluster, but the normalization in equation (1) is fitted to the observed counts in the outer pixels of a square region of 5×5 analysis pixels surrounding the pixel to be examined. To reduce correlations between neighboring pixels due to the IPC point-spread function we omit the inner (square) ring of 3×3 pixels that are adjacent to the pixel under consideration. The surface brightness of a given cluster may vary by a factor of 10 over a region of 5×5 pixels (5.33 on a side), an important limitation for this analysis. To set the physical scale of the fluctuations that we are searching for: 1′ corresponds to 20 kpc for the nearest cluster (A1060) and to 62 kpc for the most distant one (A2147). This "local" technique is not suitable for the analysis of larger scale fluctuations in the surface brightness.

For purposes of the fluctuation analysis, an azimuthally symmetric form of equation (1) was applied even to the clusters for which an overall elongation was introduced into the simulations. Because the fluctuations are measured locally, the algorithm is only weakly sensitive to the large-scale shape of the cluster. In order to account for the possibility that equation (1) fails to fit the observed cluster profile adequately, the observed fluctuations are reduced using a correction calculated for each radial ring (1′ wide) about the cluster center. The correction is the square of the difference between the average number of counts per pixel in the ring and the average number of counts per pixel calculated using the algorithm described above. The correction is on average less than 4% of the observed fluctuations. The efficiency of the fluctuation analysis technique has been tested through simulations, the results of which are described below.

The fluctuations measured over a selected area of an observed cluster are compared with the analogous quantity obtained from the simulations. Because the simulations include fluctuations due to X-ray sources outside the cluster, instrumental modulations, and Poisson fluctuations, any excess fluctuations in the observed clusters are assumed to result from intrinsic variations of the cluster surface brightness. The relative importance of instrumental modulations and Poisson noise depends strongly on the local cluster surface brightness. Accordingly, during the analysis each cluster is divided into several annuli.

Our approach is a straightforward extension of the calculation of the second moment to allow the study of nonuniform distributions. Thus, our estimator has properties similar to the second moment statistics. In particular, it is divergent for fluctuations introduced by the background sources. Since there is no *a priori* upper limit on the flux of a background source, the average fluctuation diverges. Therefore, to find if a given cluster shows intrinsic fluctuations, we determine how many of the 100 simulations produce smaller fluctuations than actually observed in the real data. If the clusters in our sample do not exhibit any intrinsic fluctuations, the fraction of simulations with fluctuations smaller than those observed would have a uniform distribution between 0 and 1. If however, the sample clusters show larger fluctuations than do the simulated clusters, this distribution will be biased toward larger fractions.

b) *Tests of the Technique*

The importance of the approximations made for the cluster simulations have been investigated for two clusters where their effects are expected to be most severe. The Coma Cluster (which produces the largest number of counts except for the Perseus Cluster and has elliptical X-ray isophotes) has been simulated without the detector modulation and the background sources. The small-scale variations present in these simulations result only from the statistical noise. In 100 simulations the average fluctuation calculated using our algorithm differ from the Poisson fluctuations by 1.5 σ in one of five radial rings, and are within 1 σ for the remaining four rings.

This implies that even for good counting statistics the algorithm does not introduce significant scatter. The same test has been applied to A2199. This cluster has an elliptical brightness distribution like the Coma Cluster, but the emission is more centrally peaked, a severe test for our fluctuation analysis algorithm. In this case, the calculated fluctuations exceed the fluctuations expected from the Poisson statistics by a factor of 2.2 in the central region between radii of 2′ and 4′. This results from the simplification in the interpolation technique in which the elongated cluster is locally approximated by an azimuthally symmetric distribution. However, since the simulated cluster is elongated like the real cluster, the artifacts introduced by the computational technique are similar for both the simulations and observations. For this reason, our statistical test is based on the difference between fluctuations in the observed and simulated clusters rather than on their absolute amount.

c) *Contributions to the Observed Fluctuations*

As an illustration of the relative magnitude of the fluctuations introduced by various effects, we summarize these for the central region of A2199 (radii 2′–4′). For simplicity, we discuss a quantity analogous to a standard deviation rather than the variance. Thus the fluctuations below correspond to the square root of the fluctuations defined above or the square root of the average square deviation between the observed (or in some cases simulated) number of counts and the smooth fits to the cluster surface brightness. In this region of A2199, the average number of counts per pixel is 109.2; thus the Poisson fluctuations are 10.4 counts per pixel. By comparing simulations of azimuthally symmetric and elliptical models of A2199, we find that neglecting the ellipticity completely would lead to fluctuations of about 11.4 counts per pixel. However, the error in our analysis is much less than this because we compare elliptical simulations to the cluster data. By comparing simulations that include the IPC modulations with those that do not, we find that the fluctuations caused by the detector are about 9.2 counts per pixel. By comparing the cluster data to the complete simulations (with elliptical cluster models), we find that the intrinsic cluster surface brightness variations and background sources together produce fluctuations of 13.8 counts per pixel.

V. RESULTS

The final sample consists of 22 observations of 20 clusters. For the Coma Cluster, observations of two regions offset from the cluster center are available in addition to the observation centered on the cluster. In each case, the area within 2′ of the cluster center is excluded from the statistical compilation since our method cannot be accurately applied to regions where the surface brightness peaks. If the emission reaches its maximum level in the test pixel, all pixels used as predictors come from regions of lower surface brightness. The central region of the Perseus Cluster (6′ radius) is also excluded since systematic errors in this region are significant (see § II). The fluctuation analysis was performed in each of 79 annuli, each centered on the peak X-ray surface brightness of the cluster under consideration. The radii of the annuli vary according to the cluster size and to the large-scale surface brightness distribution. Table 2 summarizes the dimensions and mean number of detected counts for each region.

For each annulus, the fraction of the 100 simulations exhibiting smaller fluctuations than those found in the data was determined. Figure 2 summarizes the results. No strong deviations from a uniform distribution are apparent. The apparent excess of annuli for which 95 or more simulations produced smaller fluctuations than those observed has low statistical significance. There are 11 such cases out of 79 annuli. The *a priori* probability that 11 or more would be observed for a uniform distribution is 6.9×10^{-3}. However, the probability of such an enhancement occurring in at least one bin in Figure 2 is ~ 0.14.

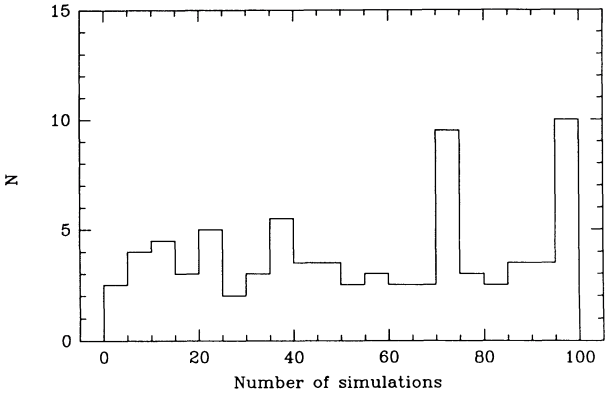

FIG. 2.—A histogram of the 79 analysis regions plotted against the number of simulations which produced smaller fluctuations than those observed. 100 simulations were performed for each region.

a) *The High- and Low-Count Samples*

Clearly our ability to detect real fluctuations depends strongly on the level of Poisson fluctuations. In Figure 3 the results of the fluctuation analysis are plotted as a function of the average number of counts per square arcminute averaged over the analysis region. As before, the results do not indicate very strong intrinsic fluctuations. In order to determine to what extent real fluctuations are masked by statistical fluctuations we divided the sample of 79 regions into two groups of 39 on the basis of the average number of counts per pixel. The region with the median number of counts per pixel (12.4) was excluded. For 24 of the 39 regions in the low-count sample more than 50% of the simulations show fluctuations larger than the observations. The opposite effect is observed in the high-count sample: in 27 of the 39 regions, fewer than 50% of the simulations show fluctuations larger than the observations.

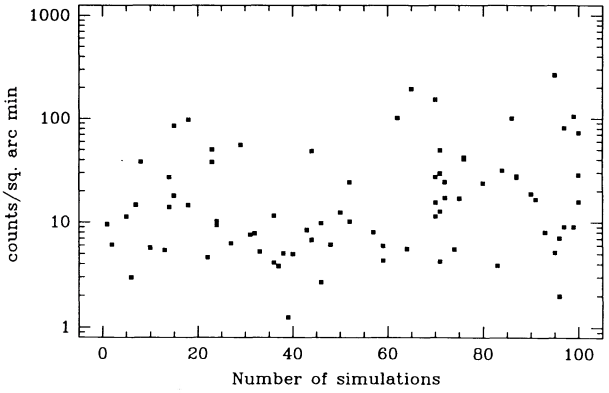

FIG. 3.—Each of the 79 analysis regions is plotted as a single point. The vertical position of the point indicates the average count density in the region; the horizontal position indicates the number of simulations producing smaller fluctuations than those observed.

TABLE 2

CHARACTERISTICS OF THE ANALYSIS REGIONS

Cluster (1)	Ring (arcmin) (2)	No. of pixels (3)	Counts per pixel (4)	Poisson Fluctuation Amplitude (5)	Total Fluctuation Amplitude (6)	1 σ upper limit of Intrinsic Fluctuation Amplitude (7)
A194	2–6	88	9.1	0.331	0.576 ± 0.029	0.506
	6–10	134	6.5	0.392	0.366 ± 0.059	0.164
	10–16	191	5.2	0.439	0.488 ± 0.063	0.334
	16–22	205	3.9	0.506	0.543 ± 0.066	0.338
A262	2–4	33	29.7	0.183	0.244 ± 0.029	0.202
	4–6	55	17.0	0.243	0.277 ± 0.024	0.178
	6–10	175	8.0	0.354	0.375 ± 0.023	0.183
	10–14	260	4.2	0.488	0.522 ± 0.029	0.256
AWM 7	2–4	33	12.4	0.284	0.310 ± 0.040	0.205
	4–8	133	5.6	0.423	0.447 ± 0.027	0.215
	8–14	358	2.0	0.707	0.797 ± 0.031	0.431
A400	2–5	58	24.6	0.202	0.250 ± 0.020	0.180
	5–10	205	11.6	0.294	0.316 ± 0.020	0.163
	10–16	344	6.2	0.402	0.463 ± 0.026	0.279
A426	6–10	176	265.1	0.061	0.106 ± 0.005	0.092
	10–16	353	108.7	0.096	0.137 ± 0.007	0.107
A496	2–4	36	81.3	0.111	0.191 ± 0.012	0.170
	4–8	126	24.3	0.203	0.226 ± 0.018	0.136
	8–12	220	9.5	0.324	0.333 ± 0.029	0.161
	12–16	214	5.2	0.439	0.460 ± 0.047	0.254
3C 129	2–6	88	27.4	0.191	0.211 ± 0.015	0.121
	6–10	175	14.7	0.261	0.254 ± 0.020	0.084
	10–16	347	8.1	0.351	0.378 ± 0.022	0.191
A539	2–4	33	15.8	0.252	0.342 ± 0.030	0.274
	4–8	133	7.1	0.375	0.451 ± 0.023	0.290
	8–10	97	3.9	0.506	0.577 ± 0.049	0.368
	10–12	126	2.6	0.620	0.634 ± 0.060	0.311
A1060	2–4	36	100.9	0.100	0.143 ± 0.013	0.120
	4–8	126	49.7	0.142	0.169 ± 0.011	0.111
	8–12	220	23.8	0.205	0.247 ± 0.012	0.158
	12–16	227	13.2	0.275	0.325 ± 0.019	0.206
A1185	2–4	36	18.8	0.231	0.294 ± 0.030	0.228
	4–8	126	11.4	0.296	0.348 ± 0.025	0.227
	8–12	217	6.8	0.383	0.419 ± 0.030	0.234
	12–16	216	5.4	0.420	0.446 ± 0.039	0.224
A1314	2–5	58	9.6	0.323	0.244 ± 0.066	...
	5–8	108	6.1	0.405	0.432 ± 0.037	0.237
	8–14	340	4.1	0.494	0.522 ± 0.022	0.228
A1367	2–4	33	85.3	0.108	0.134 ± 0.059	0.160
	4–8	114	75.8	0·115	0.485 ± 0.012	0.484
	8–12	108	53.7	0.136	0.188 ± 0.053	0.199
	12–18	195	39.9	0.158	0.187 ± 0.068	0.222
	18–24	176	31.5	0.178	0.326 ± 0.043	0.323
A1656	2–4	33	195.1	0.072	0.130 ± 0.012	0.123
	4–6	55	153.7	0.081	0.124 ± 0.010	0.107
	6–10	175	98.0	0.101	0.123 ± 0.007	0.082
	10–16	345	43.2	0.152	0.192 ± 0.009	0.131
	16–22	161	13.9	0.268	0.259 ± 0.021	0.080
	22–28	167	7.9	0.356	0.365 ± 0.025	0.169
	28–34	150	6.4	0.395	0.402 ± 0.048	0.215
	18–26	206	9.7	0.321	0.357 ± 0.079	0.295
	26–21	165	9.6	0.323	1.253 ± 0.164	1.380
	32–40	163	5.6	0.423	0.609 ± 0.042	0.495
A1736	2–5	58	31.8	0.177	0.214 ± 0.019	0.151
	5–8	100	17.8	0.237	0.269 ± 0.036	0.192
	8–14	237	10.3	0.312	0.337 ± 0.068	0.259
	14–20	202	8.4	0.345	0.710 ± 0.061	0.689

TABLE 2—*Continued*

Cluster (1)	Ring (arcmin) (2)	No. of pixels (3)	Counts per pixel (4)	Poisson Fluctuation Amplitude (5)	Total Fluctuation Amplitude (6)	1 σ upper limit of Intrinsic Fluctuation Amplitude (7)
A2052	2– 4	33	14.7	0.261	0.280 ± 0.046	0.196
	4– 8	133	4.3	0.482	0.505 ± 0.031	0.234
	8–16	453	1.3	0.877	0.904 ± 0.057	0.393
A2063	2– 5	58	28.6	0.187	0.275 ± 0.017	0.224
	5– 8	108	10.2	0.313	0.334 ± 0.024	0.171
	8–12	223	4.6	0.466	0.462 ± 0.039	0.183
	12–16	270	3.0	0.577	0.528 ± 0.094	0.231
A2147	2– 4	36	50.7	0.140	0.165 ± 0.029	0.134
	4– 8	126	27.2	0.192	0.242 ± 0.015	0.171
	8–12	214	18.0	0.236	0.234 ± 0.020	0.095
	12–16	201	11.2	0.299	0.296 ± 0.036	0.145
ZW 1615+35	2– 6	86	7.6	0.363	0.372 ± 0.034	0.182
	6–10	149	5.8	0.415	0.398 ± 0.039	0.136
	10–16	251	5.5	0.426	0.468 ± 0.036	0.269
A2199	2– 4	33	105.2	0.097	0.216 ± 0.015	0.209
	4– 6	55	42.3	0.154	0.211 ± 0.016	0.167
	6–10	175	15.5	0.254	0.285 ± 0.018	0.165
	10–16	336	5.8	0.415	0.481 ± 0.076	0.371
A2634	2– 4	33	55.9	0.143	0.162 ± 0.043	0.155
	4– 6	55	38.6	0.161	0.162 ± 0.061	0.154
	6–10	175	27.3	0.191	0.295 ± 0.030	0.263
	10–16	350	17.5	0.239	0.387 ± 0.040	0.354

Figure 4 illustrates the cumulative distributions of the two samples. The Kolmogorov-Smirov (K-S) test has been applied to evaluate the significance of the results noted above. The K-S test indicates that the distribution of the low-count sample does not deviate significantly from a uniform distribution. The high-count sample, however, differs from the uniform distribution at 0.9991 confidence. The two-sample K-S test indicates that the probability that the two samples are drawn from the same parent population is 0.0059. We thus infer that some intrinsic fluctuations are detected in the regions where the statistical signal-to-noise is best, although the effect is not strong. Furthermore, the reality of this result depends on the accurate simulation of the modulations introduced by the IPC. Our result applies to the high-count sample as a whole; we can say only that fluctuations in the high-density subsample are on the average larger than fluctuations due to background sources and instrumental effects without singling out individual clusters.

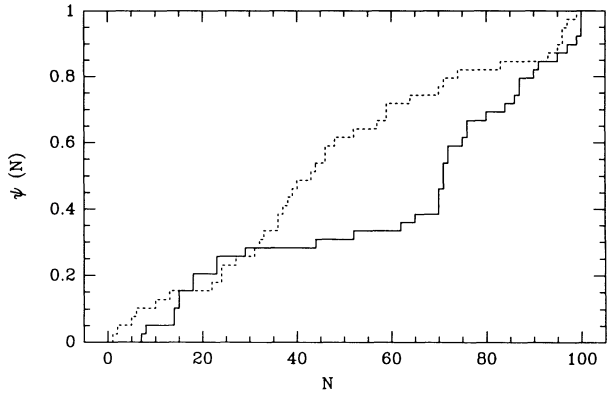

FIG. 4.—The cumulative distributions of the 39 regions with a high-count density (*solid line*) and the 39 regions with a low-count density (*broken line*). $\Psi(N)$ is the fraction of regions in which the observed fluctuations exceed the fluctuations in N simulations. The two-sample K-S test shows that the two distributions differ at a confidence level of 0.9941.

b) Amplitude of the Fluctuations in the High-Count Sample

However, even though our apparent detection of excess fluctuations is a statistical statement that applies to our high-count sample as a whole, it is important to consider the sensitivity of our analysis and to determine approximately the amplitude of the fluctuations that we detect. We consider two aspects of this issue: (1) What are the magnitudes of the fluctuations measured in each analysis region and the uncertainties in these numbers? (2) What source luminosities are required to explain the fluctuations observed in the high-count sample?

With regard to the first issue, it is obvious that Poisson noise sets the ultimate lower limit to the amplitude of the observable fluctuations. However, because other factors contribute to the fluctuations, we estimate the uncertainties in the observed fluctuations by means of simulations similar to those described in § III. Because the objective is to estimate the uncertainties of the measured fluctuations and not the *a priori* expected average fluctuations, we introduce a maximum flux cut-off in the log N-log S relation for the background sources at the level of the brightest pointlike source detected in a given observation. We define the fluctuation amplitude in a given region to be the ratio of the square root of the observed fluctuations to the average counts per pixel; this quantity is listed for each of the 79 regions in column (6) of Table 2. The standard deviation of the fluctuation amplitude in each region has been estimated from 100 simulations; these values are given in column (7) of

Table 2. The expected relative fluctuation amplitudes implied by the Poisson statistics (the second moment of the distribution or approximately the inverse square root of the average counts per pixel) are given in column (5) of Table 2. These are on the average smaller than the observed amplitudes because effects other than the Poisson noise contribute to the fluctuations. Unfortunately, the amount by which the fluctuations exceed the Poisson noise in a given zone cannot be used directly to determine the magnitude of the intrinsic cluster surface brightness variations because the excess may be due to intrinsic fluctuations, background sources, or instrumental modulations. However, an upper limit to the intrinsic fluctuations can be derived in each region from these numbers; the 1 σ limit for each region is plotted in column (8) of Table 2. In regions containing a strong background source, e.g., the seventh of the 10 Coma Cluster regions which contains X Comae, this limit is quite weak.

To help determine what source properties are required to produce the excess fluctuations observed in the high-count sample, we have produced two histograms of the count distributions in the 4221 pixels included in 36 of the 39 regions in the high-count sample. (The central regions of A426, A496, and A2199 have been excluded for reasons discussed below.) One histogram plots the difference between the observed counts per pixel and the number predicted from a smooth cluster model as discussed in § IV. The other histogram plots the difference between the counts per pixel in the simulated observations of smooth clusters and the number predicted from the smooth cluster model. In order to allow a single histogram to include all 4221 pixels, the count differences in each pixel have been normalized to the Poisson standard deviation estimated from the smooth cluster models. The two histograms are plotted in Figure 5. The histogram produced from the observations is slightly broader than the histogram produced from the simulations. The majority of the excess width results from ~ 60 positive fluctuations of size 1.0–3.5 standard deviations, or ~ 1–2 per region.

Motivated by these histograms of count differences, we consider here the simple case where the excess fluctuations are dominated by a single source per region, and determine the approximate luminosity of the sources responsible for the excess fluctuations. We have repeated the fluctuation analysis for two clusters in the high-count sample, adding an unresolved source of fixed luminosity to each region of the simulated (comparison) clusters. Two clusters with approximate azimuthal symmetry but lying at the extremes of our redshift range were chosen: A1060 (nearby) and A2634 (distant). Using the data plotted in Figure 3, we estimate that the high-count sample would be distributed uniformly if the number of simulations with fluctuations smaller than the observed fluctuations were increased by $\sim 10\%$. This change can be produced by adding a single unresolved source to each analysis region of luminosity $\sim 8 \times 10^{40}$ ergs s^{-1} in A1060 and $\sim 7 \times 10^{41}$ ergs s^{-1} in A2634. The effect of adding a source of fixed luminosity depends on the local cluster surface brightness and the observation length as well as the cluster distance, but the luminosities given here should be representative.

c) *Regions with Large Fluctuations*

We now return to the apparent excess of cluster regions in which the observed fluctuations are larger than those in at least 95% of the simulations. For a uniform distribution one should expect approximately four such cases, as compared with the 11 observed. The regions where these comparatively strong fluctuations are detected span a wide range of surface densities. Five of these regions are in the low-count sample and six are in the high-count sample. We have examined these 11 regions further to determine the origin of the fluctuations.

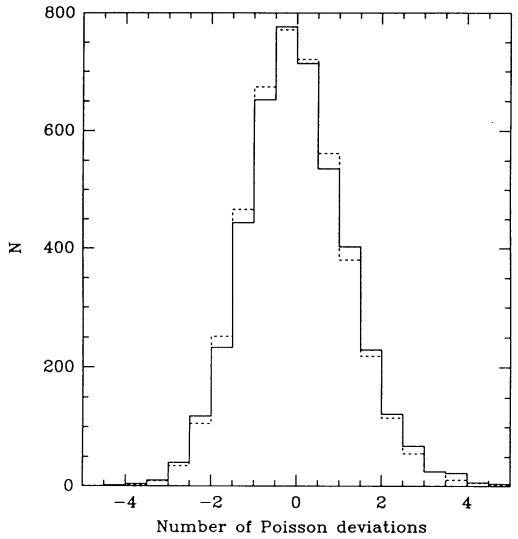

FIG. 5.—The solid line is the histogram of the difference between the observed number of counts and the number predicted in a smooth cluster model in each of 4221 pixels in the 39 high-count regions. The broken line is the histogram and the difference between the number of counts in simulated observations of smooth clusters and the smooth cluster models in the same 4221 pixels. The count differences have been normalized to the Poisson deviation estimated from the predicted count distribution.

Seven regions contain strong unresolved sources which are responsible for the excess fluctuations. The positions of four of these sources can be identified with individual galaxies: NGC 545/NGC 547 (3C 40) in A194, a galaxy in A539 ($\alpha = 5^h13^m45^s.7$, $\delta = +6°25'7''$, 1950.0), NGC 3862 (3C 264) in A1367 and a Zwicky galaxy (actually a close pair of galaxies) in A2063 ($\alpha = 15^h20^m46^s.3$, $\delta = +8°43'37''$, 1950.0). The identifications have been verified using HRI observations excepting NGC 545/NGC 547, for which no HRI data are available. HRI positional errors are less than or equal to 5″; IPC positional errors are $\sim 1'$. The HRI positions are given above. The 0.3–3.5 keV luminosities of these sources are respectively: $4.5 \pm 1.0 \times 10^{41}$, $8.0 \pm 3.2 \times 10^{41}$, $4.0 \pm 0.2 \times 10^{42}$, and $3.4 \pm 0.9 \times 10^{42}$ (but see below) ergs s^{-1}. The errors here are based on counting statistics; see § II for a discussion of the uncertainties associated with conversion of IPC counts to flux. The source associated with NGC 3862 has been previously discussed by Elvis *et al.* (1981). Another two of these sources are apparently coincident with background sources (X Comae and 5C 4.105 in the Coma Cluster fields). The remaining source in A539 has no obvious optical counterpart.

In the remaining four of the 11 regions no obvious sources are detected. In three of the four (A426, A496 and A2199), the excess fluctuations seem to result from significant ($\sim 30\%$) azimuthal variations of the surface brightness at distances of $\sim 2'$–$4'$ ($\geq 6'$ for A426) from the cluster center, indicating that simple azimuthally symmetric or elliptical models are in some cases inadequate. The limited angular resolution of our data prevents accurate characterization of these deviations, but it is clear that distinct irregularities in the cluster surface brightness

occur very close to the cluster center in A496 and A2199. Abell 426 (the Perseus Cluster) exhibits a well-known dipole-type asymmetry: the center of the high surface brightness region of $\sim 5'$ radius is displaced by $\sim 1'.5$ from the center of the outer part of the cluster (Branduardi-Raymont *et al.* 1981). The fourth of the 11 regions lies in the outskirts (8′–14′ radius) of AWM 7. This is a low-exposure observation producing an average of ~ 2 counts per pixel in the annulus in question. Several pixels contribute to the observed fluctuations, but the large Poisson noise does not permit us to identify particular local enhancements as the source of the fluctuations.

d) The Final High-Count Sample

In view of the probability that the central regions of three clusters (A426, A496, and A2199) show strong fluctuations due to departures from asymmetry rather than from pixel-to-pixel variations of the surface brightness, the statistical analysis using the K-S test has been repeated with these three regions excluded. The high-count group (which now contains 36 regions) shows the presence of intrinsic fluctuations although at lower significance level. The cumulative distribution of the fraction of simulations exhibiting smaller fluctuations than those observed (as described previously) differs from the uniform distribution at 0.994 confidence and the probability that the high-count and low-count samples are drawn from the same parent distribution is 0.0086.

e) Clusters with Repeated Observations

Our sample contains three clusters (divided into 12 analysis regions) for which two *Einstein* observations are available: A496, A2063, and A2634. In the statistical investigation described previously, we used only the longer observation. In order to evaluate the internal consistency of our calculations, the shorter observations have also been analyzed. In each of the 12 regions the difference between the fluctuations found in the two observations is compared with the uncertainty of the fluctuation determinations given in column (5) of Table 2. In nine regions the calculated differences are within these uncertainties, in two regions the differences exceed the uncertainties by a factor of ~ 1.5, but in one region (the inner ring of A2063) the differences exceed the uncertainties by a factor of 3.2. Thus, there is a good agreement between the two sets of observations with the exception of the central region of A2063, which we discuss further below.

VI. DISCUSSION

We turn now to the four sources associated with cluster galaxies, because these detected sources with luminosities between 4.5×10^{41} and 4.0×10^{42} ergs s^{-1} likely provide the best indication as to the nature of the sources (with luminosities near the lower end of this range) that could produce the excess fluctuations in the high-count sample. As noted previously, HRI observations exist for three of these four sources (NGC 545/NGC 547 is the exception). In each case, a source unresolved by the HRI is found, indicating source extents less than or equal to 2″–3″. This fact, coupled with the luminosities of these sources, suggests that we are in fact observing low-luminosity AGN. In fact, Stauffer (1981) classifies the galaxy in A539 as a Seyfert Type I, with an Hα luminosity of $\sim 10^{40}$ ergs s^{-1}.

In further support for the identification of these sources as low-luminosity AGN, the source in A2063 is apparently variable. The discrepancy between the two sets of observations alluded to above results from a strong positive signal at the source position in the longer observation carried out on 1979 February 5. Using the standard *Einstein* IPC (LDETECT) source detection algorithm an unresolved source with a flux of $(9.4 \pm 2.5) \times 10^{-13}$ ergs cm^{-2} s^{-1} is detected. As mentioned above, this source is also visible in an HRI observation on 1979 August 23. However, during the shorter of the two *Einstein* IPC observations on 1979 January 24, no source is detected with a 3 σ upper limit of 7.5×10^{-13} ergs cm^{-2} s^{-1}. The data thus suggest the presence of a source with a variability time scale of ~ 10 days. (The source luminosity during the second IPC observation is $\sim 3.4 \times 10^{42}$ ergs s^{-1} as given above.)

Is it plausible that all the fluctuations we detect are consistent with the contributions of low-luminosity AGN? It is impossible to answer this question unambiguously given the present very uncertain census of low-luminosity AGN overall, and the further uncertainties of the influence of the cluster environment. However, we have examined two clusters, A262 and A2634, which contain two and four regions in the high-count sample respectively, and for which J and F band galaxy photometry is available (Butcher and Oemler 1985). Taking $B-J = 0.4$, we find four galaxies in A262 and 22 galaxies in A2634 with $M_B \leq -19.5$ within the high-count sample regions. According to the prescription in § I, we would expect less than or equal to 25% of these to emit greater than or equal to 10^{41} ergs s^{-1} in the 0.5–4.5 keV, or equivalently (within $\sim 20\%$ accuracy) the 0.3–3.5 keV band. At the (rather unlikely) upper end of this estimate, we come rather close to producing the required one source per region with the appropriate luminosity, and explaining all the fluctuations in the high-count sample with low-luminosity AGN.

However, we recall the nine extended ($\sim 1'$ extent) sources associated with galaxies in A1367 detected by Bechtold *et al.* (1983) with luminosities exceeding 10^{41} ergs s^{-1}. These fall within five high-count regions in our sample. Such sources of extended emission, presumably associated with hot gas in individual galaxies, may well contribute to the observed fluctuations in our sample in clusters other than A1367. A more complete understanding of the relative importance of these two types of sources in clusters, as well as the detection of more subtle features must await an X-ray observatory like *AXAF* that combines considerably more sensitivity than the *Einstein Observatory* with high angular resolution.

A. S. is grateful to H. Tananbaum and the High Energy Astrophysics Division for hospitality during his stay at the CfA and acknowledges support from NASA contract NAS8-30751. We thank Martin Elvis, Pepi Fabbiano, and Jules Halpern for helpful discussions concerning the X-ray emission from normal and active galaxies, and Simon White for renewing our interest in this project and for several incisive comments on the manuscript.

REFERENCES

Abell, G. 1958, *Ap. J. Suppl.*, **3**, 211.
Bechtold, J., Forman, W., Giacconi, R., Jones, C., Schwarz, J., Tucker, W., and Van Speybroeck, L. 1983, *Ap. J.*, **265**, 26.
Branduardi-Raymont, G., Fabricant, D., Feigelson, E., Gorenstein, P., Grindlay, J., Soltan, A., and Zamorani, G. 1981, *Ap. J.*, **248**, 55.
Butcher, H., and Oemler, A., Jr. 1985, *Ap. J. Suppl.*, **57**, 665.
Canizares, C. 1988, in *Cooling Flows in Clusters and Galaxies*, ed. A. Fabian (Dordrecht: Kluwer), p. 376.
Canizares, C., Fabbiano, G., and Trinchieri, G. 1987, *Ap. J.*, **312**, 503.
Dressler, A., Thompson, I., and Shectman, S. 1985, *Ap. J.*, **288**, 481.

Elvis, M., Schreier, E., Tonry, J., Davis, M., and Huchra, J. 1981, *Ap. J.*, **246**, 20.
Elvis, M., Soltan, A., and Keel, W. 1983, *Ap. J.*, **283**, 479.
Dressler, A., and Shectman, S. 1988, *A.J.*, **95**, 985.
Fabbiano, G., 1989, *Ann. Rev. Astr. Ap.*, **27**, 87.
Forman, W., and Jones, C. 1990, private communication.
Forman, W., Bechtold, J., Blair, W., Giacconi, R., Van Speybroeck, L., and Jones, C. 1981, *Ap. J. (Letters)*, **243**, L133.
Geller, M., and Beers, T. 1982, *Pub. A.S.P.*, **94**, 421.
Gioia, I., Maccacaro, T., Schild, R., Stocke, J., Liebert, J., Danzinger, I., Kunth, D., and Lub., J. 1984, *Ap. J.*, **283**, 495.
Gioia, I., Maccacaro, T., Schild, R., Wolter, A., Stocke, J., Morris, S., and Henry, J. 1990, *Ap. J. Suppl.*, **72**, 567.
Halpern, J., and Steiner, J. 1983, *Ap. J. (Letters)*, **269**, L37.
Harnden, F. R., Jr., Fabricant, D., Harris, D., and Schwarz, J. 1984, SAO Spec. Rept. No. 393.
Heckman, T. 1980, *Astr. Ap.*, **87**, 152.
Hertz, P., and Grindlay, J. 1984, *Ap. J.*, **278**, 137.
Jones, C., and Forman, W. 1990, in preparation.
Keel, W. 1983, *Ap. J. Suppl.*, **52**, 229.
Persic, M., De Zotti, G., Danese, L., Palumbo, G., Franceschini, A., Boldt, E., and Marshall, F. 1989, *Ap. J.*, **344**, 125.
Stauffer, J. 1981, Ph.D. thesis, University of California at Berkeley.
Wu, X., Hamilton, T., Helfand, D., and Wang, Q. 1990, submitted to *Ap. J.*

DANIEL G. FABRICANT: Harvard-Smithsonian Center for Astrophysics, 60 Garden Street, Cambridge, MA 02138

ANDRZEJ SOLTAN: Polish Academy of Sciences, Copernicus Astronomical Center, Bartycka 18, 00-716 Warsaw, Poland